2024 IEEE International Conference on Robotics and Automation (ICRA 2024)
May 13-17, 2024. Yokohama, Japan

Thin-film NiTi Microactuator With A Magnetic Spring For A Tiny Launcher Mechanism

Sukjun Kim[1*], Sarah Bergbreiter[2]

Abstract— **In this work, we present a thin-film shape memory alloy microactuator with a magnetic spring. This novel actuator design utilizes two permanent magnets and 3D-printed magnet holders to effectively apply a tensile strain on the NiTi thin-film. This actuator is expected to generate 8.7 mN of blocking force, and a free displacement of 30 μm is experimentally characterized. The actuator leverages bare NiTi film ($\sim$ 1 μm thick) for actuation, enabling a high actuator bandwidth up to 50 Hz. A comprehensive analytical model is also studied, which was then validated by comparing to the experimental results. A launcher mechanism was designed and integrated with the NiTi actuator, and this mechanism was used to launch a microscale projectile (a salt grain) thereby demonstrating the relative high power actuation achievable with thin-film NiTi.**

I. INTRODUCTION

Microactuators capable of providing a large amount of mechanical work are necessary for small-scale robotic systems due to limitations in size and mass. Among various microactuation methods, shape memory alloy (SMA) is an attractive actuation option for microrobots, as it can take advantage of high-work density materials such as NiTi ($\sim$ 1 J/g) to provide a high force and a large displacement. NiTi thin films ($< 5\,\mu$m) can also be microfabricated using sputter deposition processes for microscale applications [1]–[4].

One of the major challenges of using NiTi is that the NiTi needs to be strained prior to actuation. The applied strain (up to 5%) detwins NiTi in the martensite (low temperature) phase, and then a large amount of work can be produced when the NiTi recovers to its original shape when heated. At larger scales, various methods have been implemented to apply a strain to SMA actuators, since mechanical structures can be easily manufactured and integrated with NiTi materials such as weights [5], springs [6], [7], and antagonistic SMA actuators [8], [9]. However, applying strain to NiTi thin films has remained a significant challenge due to limited manufacturing and integration approaches at the microscale.

The most common approach to apply an initial strain to microfabricated NiTi is the inclusion of a passive material laminated with the NiTi to create a bilayer structure. Residual stress from passive layers made from materials such as silicon [2], metal [1], and polymer [3], [4], [10], [11] bend the bilayer actuators, thus applying strain to the NiTi layer. Although this approach has been most favorable because of its simple and robust fabrication, the strain induced within the NiTi film when bent is highly limited and the passive layer also increases the thermal mass of the actuator, slowing down the actuation speed ($<$ 4.3 Hz in [11]). Another approach has focused on manually bending a NiTi actuator using a micromanipulator [12]. Despite the simplicity of this approach, the amount of strain applied to the NiTi thin film was limited and difficult to control. The NiTi actuator also needs to be manually deformed every time before actuation, making this approach less practical for microrobotic applications. A final approach found in the literature utilized a mechanical spring or a pressurized fluid to strain the thin-film NiTi [13], [14]. This method requires complicated assembly processes to align the spring or keep the fluid inside the chamber.

In this work, a novel thin-film NiTi microactuator with a magnetic spring is demonstrated for the first time. The magnetic force between two permanent magnets is utilized to apply a tensile strain on thin-film NiTi. The combination of NiTi and a magnetic spring has been previously studied at the larger scale [15], but has not been achievable at smaller scales due to a variety of material and fabrication challenges. Perhaps the most critical challenge for using permanent magnets at the microscale has been a lack of manufacturing methods for creating 3D structures to hold magnets at desired positions in 3D space.

A primary contribution of this work is a demonstration of a magnetic spring at the microscale using 3D printing with two-photon polymerization (TPP). TPP enables direct laser writing of complex microstructures in 3D space and has been used to successfully demonstrate 3D-printed microactuators [16], [17] and microrobots [11], [18]–[20]. 3D-printed magnet holders as shown in Fig. 1 are utilized to hold magnets in 3D space. Since this approach can leverage bare thin-film NiTi for actuation without any added passive layers, the actuator can be operated at high frequencies up to 50 Hz. A secondary contribution of this work is a comprehensive modeling and experimental characterization of the thin-film NiTi actuator. An electro-thermo-mechanical model of the NiTi actuator was built, and the transient characteristics were experimentally evaluated and compared with the model. A third contribution is a launcher mechanism driven by the thin-film NiTi microactuator. By 3D printing and integrating the linkage mechanism with the actuator, the launcher was able to launch a projectile (a salt grain) demonstrating the powerful actuation from the novel thin-film NiTi actuator with a magnetic spring.

This work was supported by the Presidential Fellowship from Carnegie Mellon University

[1]Sukjun Kim is with the Mechanical and Aerospace Engineering, University of California, San Diego, La Jolla, CA 92093 USA (e-mail: suk056@ucsd.edu)

[2]Sarah Bergbreiter is with the Department of Mechanical Engineering, Carnegie Mellon University, Pittsburgh, PA 15213 USA (e-mail: sbergbre@andrew.cmu.edu)

* Corresponding author

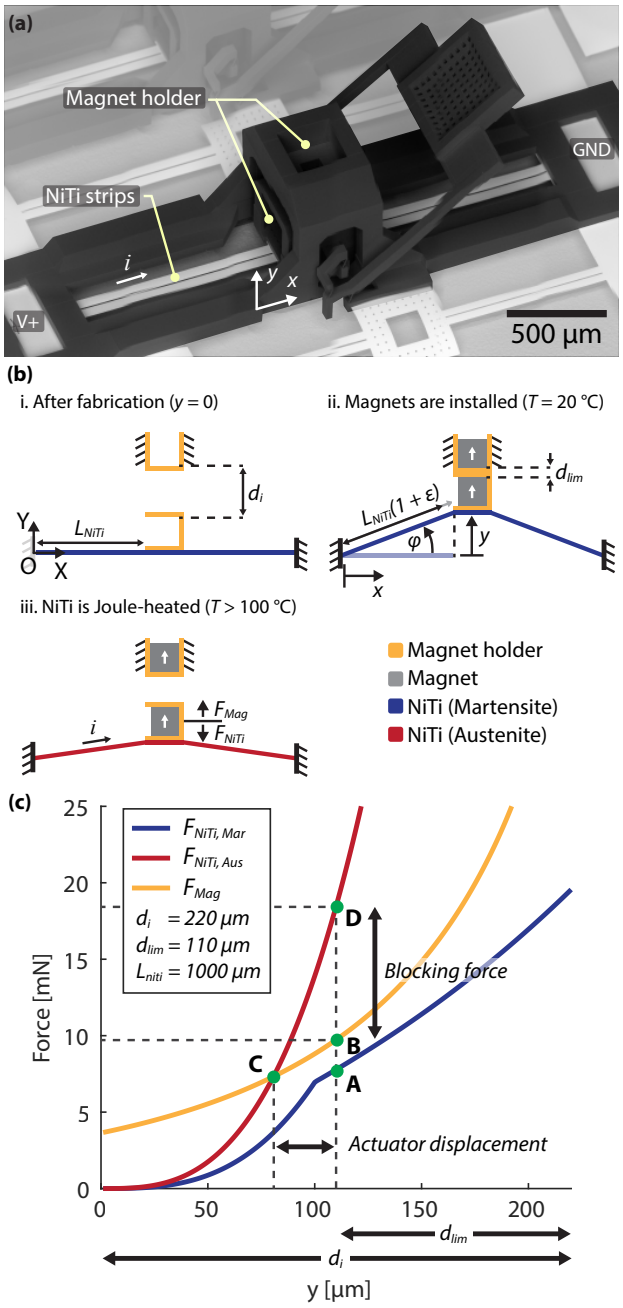

Fig. 1. Design and working principle of the thin-film NiTi actuator with a magnetic spring. (a) A scanning electron microscopy of the actuator without magnets. (b) A working principle of the actuator. The magnetic force between two magnets applies a tensile strain on the thin-film NiTi. When the actuator is heated up, the thin-film NiTi undergoes the phase transformation and moves the actuator. (c) An analytically modeled force-displacement profile of the NiTi actuator and the magnetic force.

II. METHODS

A. Design

In order to leverage the shape-memory effect and achieve a large work output from NiTi, a pre-strain needs to be applied to the thin-film NiTi. In this work, we 3D-printed magnet holders to keep the magnets in place so that the magnetic force can apply a tensile strain to the NiTi strips (Fig. 1(a)). As shown in Fig. 1(b)-i, strips of thin-film NiTi are clamped to the substrate at both ends, and a magnet holder is placed in the middle of the NiTi strips. The NiTi length between the clamped end and the magnet holder is L_{NiTi}. The other magnet holder is mechanically fixed above so that the initial distance between the surfaces of the two magnets is d_i in the Y-direction. After permanent magnets are installed into the magnet holders (Fig. 1(b)-ii), the NiTi strips are pulled upward due to the magnetic force, and a tensile strain is applied to the NiTi strips. The actuator position is defined here as y. The magnet holders are designed to maintain a minimum distance of d_{lim} between two magnets. When a current is applied to the NiTi for Joule heating and the temperature of the NiTi strips (T) exceeds the phase transition temperature, the phase of the NiTi changes from martensite to austenite, and the NiTi strips can recover their original flat shape. As a result, the actuator moves down along the Y-axis as shown in Fig. 1(b)-iii.

Fig. 1(c) shows the modeled force-displacement profiles of each component of the actuator. A detailed modeling of the actuator will be discussed in Section II-B. F_{NiTi} and F_{Mag} are the force from the NiTi strips and the magnetic force between two permanent magnets (Fig. 1(b)-iii). *Mar* and *Aus* represent the martensite and austenite phases of NiTi, respectively. At room temperature (T = 20 °C), NiTi is fully in the martensite phase, and $F_{NiTi,Mar}$ shows a change in slope due to detwinning. Since F_{Mag} is always greater than $F_{NiTi,Mar}$, the magnetic force can pull the NiTi strips up to the maximum actuator position, $y = d_i - d_{lim}$. Therefore, the equilibrium position of the NiTi actuator in the martensite phase is at point **A** in Fig. 1(c). When the NiTi strips start to heat up as a result of the applied current, the phase of NiTi partially changes to austenite. F_{NiTi} then gradually increases by following the line from point **A** to point **B**. Once F_{NiTi} reaches point **B**, F_{NiTi} can move the actuator and follow the orange line from point **B** to point **C**. When the NiTi is in full austenite phase (T > 100 °C), the equilibrium position of the actuator is at point **C** where $F_{NiTi,Aus}$ and F_{Mag} cross. Therefore, the displacement between points **B** and **C** is the no-load displacement of the actuator, which is modeled at 29 μm. When the actuator is blocked and cannot move, F_{NiTi} follows the line between points **B** and **D**. The force difference between the point **B** and **D** is the expected blocking force, which is estimated to be 8.7 mN. The actuator design parameters are listed in Table I.

To demonstrate the high power actuation of the NiTi microactuator, a launcher mechanism is designed and integrated as shown in Fig. 2(a). Fig. 2(c) shows the schematics of the launcher mechanism. The magnet holder centered on the NiTi strips can only translate in the Y-axis. To launch the projectile at an angle, this magnet holder is connected to the green base link which is connected to the blue seesaw-like link that is pivoted in the middle. An offset, y_i, is added between the magnet holder and the pivot point. This mechanism translates the actuator's input linear motion to the launcher's output rotary motion. Cross-spring pivot flexure joints [21] are used in place of pin joints between links as

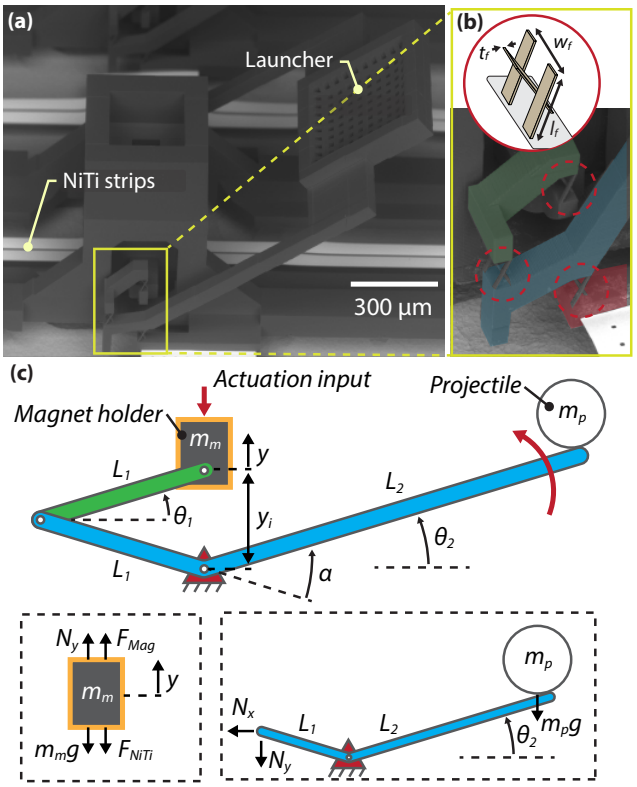

Fig. 2. Design and modeling of the launcher mechanism. (a) A scanning electron microscopy of the actuator and the launcher. The links are connected via cross-pivot flexure joints. (b) Schematic and SEM image of flexure joints. (c) A schematic and free body diagrams of the launcher mechanism.

TABLE I

LIST OF THE DESIGN PARAMETERS

L_{NiTi}	1000 µm	L_1	150 µm	l_f	67 µm
w_{NiTi}	100 µm	L_2	1000 µm	w_f	25 µm
t_{NiTi}	1 µm	y_i	180 µm	t_f	2 µm
d_i	220 µm	α	38 °	-	
d_{lim}	110 µm	g_{si}	60 µm	-	

shown in the Fig. 2(b) since flexure joints provide useful characteristics at the smaller scale such as zero friction and zero joint backlash. Each link of the mechanism is color-coded in Fig. 2 for better visualization.

B. Modeling

Studying an analytical model of the actuator and the mechanism is important as the model allows us to simulate and design a desired actuated mechanism. First, we can calculate the change in the temperature on the NiTi strips ($T(t,x)$) when a step current of i is applied by solving Eq 1. t is time, and x indicates the position on the NiTi strips along X-axis as shown in Fig. 1(b)-ii. The relevant design and material variables are listed in Table I and Table II.

TABLE II

LIST OF THE MATERIAL PROPERTIES USED IN THE MODEL

C_{NiTi}	3700 $\mathrm{Jkg^{-1}K^{-1}}$	E_{Aus}	140 GPa
d_{NiTi}	6450 $\mathrm{kgm^{-3}}$	E_{Mar}	70 GPa
k_{NiTi}	10 $\mathrm{Wm^{-1}K^{-1}}$	σ_s^{crit}	350 MPa
ρ_{NiTi}	2.4 $\times 10^{-6}$ Ωm	σ_f^{crit}	600 MPa
h_{air}	25 $\mathrm{Wm^{-2}K^{-1}}$	T_s^{aus}	60°C
k_{air}	0.026 $\mathrm{Wm^{-1}K^{-1}}$	T_f^{aus}	110°C

$$C_{NiTi}d_{NiTi}\frac{\partial T}{\partial t} = k_{NiTi}\frac{\partial^2 T}{\partial x^2} + J_{den}^2\rho_{NiTi} - \frac{h_{air}P_{NiTi}}{A_{NiTi}}T - \frac{k_{air}P_{NiTi}F_s}{A_{NiTi}g_{si}}T \quad (1)$$

where we assumed the initial conditions of $T(0,x) = T(t,0) = T(t,2L_{NiTi}) = 20°\mathrm{C}$ for all t and x. The magnet holder in the middle of the NiTi strips is not considered in the model. C_{NiTi}, d_{NiTi}, k_{NiTi}, ρ_{NiTi} are the specific heat capacity, density, thermal conductivity, and resistivity of NiTi, respectively. P_{NiTi} and A_{NiTi} are the perimeter and cross sectional area of the NiTi strips, which are $2w_{NiTi} + 2t_{NiTi}$ and $w_{NiTi}t_{NiTi}$. J_{den} is the current density which is i/A_{NiTi}. h_{air} and k_{air} are the convection coefficient and thermal conductivity of air. g_{si} and F_s are the gap between the NiTi strips and Silicon substrate underneath and the shape factor of the NiTi strips [22], respectively. The average temperature of the NiTi strips at time t (T_{avg}) can be then calculated by

$$T_{avg}(t) = \frac{1}{2L_{NiTi}}\int_0^{2L_{NiTi}} T\,dx \quad (2)$$

Secondly, the amount of force generated by the NiTi actuator (F_{NiTi}) can be calculated. When the actuator is vertically displaced by y as shown in Fig. 1(b), the tensile strain (ε) on the NiTi strips is

$$\varepsilon = \frac{\sqrt{(L_{NiTi}+y)^2} - L_{NiTi}}{L_{NiTi}} \quad (3)$$

Given the strain (ε) and the temperature (T_{avg}), the Brinson model [23] was used to calculate the stress on the NiTi strips (σ) by using the material properties of NiTi in Table II. E_{Aus} and E_{Mar} are the Young's modulus of NiTi when fully in austenite and martensite phases. σ_s^{crit} and σ_f^{crit} are the critical stresses when the detwinning of NiTi starts and ends. T_s^{aus} and T_f^{aus} are the temperature when the martensite to austenite phase transition starts and finishes. We assumed that the phase-transition temperatures do not change with respect to the applied stress. Therefore, F_{NiTi} is

$$F_{NiTi} = 2\sigma A_{NiTi}\sin\varphi, \quad \varphi = \sin^{-1}\left(\frac{y}{L_{NiTi}(1+\varepsilon)}\right) \quad (4)$$

where φ is the angle between the substrate and the NiTi strips (Fig. 1(b)-ii).

Third, the force between two permanent cube magnets was analytically determined by the model from [24] using the distance between two magnets of $d_i - y$. The remanence (Br) was assumed to be 1.43 T for N50 magnets.

Lastly, a dynamic model of the launcher mechanism was also studied. Fig. 2(c) shows the schematic and free body diagrams of the launcher mechanism. Since the mass of the magnet on the NiTi strip (m_m) and the projectile (m_p) are much greater than the mass of the links, massless links are assumed in the model. The stiffness of the flexure joint was also assumed to be negligible. Four force components are applied to the moving magnet m_m in Y-axis.

$$m_m\ddot{y} = N_y + F_{Mag} - m_m g - F_{NiTi} \tag{5}$$

where N_y is the vertical reaction force from the green link to m_m, and g is gravity. The forces applied to the blue link by the green link should satisfy the following equation.

$$N_y = N_x \tan\theta_1 \tag{6}$$

We consider the moment equilibrium around the pivot point for the blue link.

$$m_p L_2^2 \ddot{\theta}_2 = N_y L_1 \cos\theta_1 + N_x L_1 \sin\theta_1 - m_p g L_2 \cos\theta_2 \tag{7}$$

From the geometric constraint,

$$\theta_1 = \sin^{-1}\left(\frac{y_i + y}{2L_1}\right), \quad \theta_2 = \alpha - \theta_1 \tag{8}$$

where α is the angle on the blue link as shown in Fig. 2(c). By solving Eq. 5 and 7, the position of the actuator (y), the launcher angle (θ_2), and the projectile velocity (v_{proj}) and height (h_{proj}) can be calculated. When the normal force applied to the projectile by the blue link goes to zero, the projectile takes off from the launcher.

C. Fabrication

A fabrication process for the NiTi actuator and the launcher is based on the method previously demonstrated in [10], [11] which combines microfabrication with 3D printing to create more complex 3D actuators and mechanisms. First, a thin film of NiTi was co-sputtered on a silicon wafer, and ion milling was utilized to pattern the NiTi film. The wafer was then diced, and the magnet holders and launcher mechanism were directly 3D-printed over the NiTi layer using two-photon polymerization with IP-S photoresist (Nanoscribe Photonic Professional GT +, Nanoscribe Gmbh). The NiTi strips and mechanisms were released from the substrate with XeF_2 (SPTS Xactix, Xetch). Finally, two 250 µm cube magnets (N50, Supermagnetman) were manually inserted into the magnet holders with their poles aligned.

III. RESULTS

A. Thin-film NiTi actuator characterization

The temperature of the NiTi strips needs to be higher than the phase transition temperature during actuation to take advantage of the shape memory effect. Similar to previous works [10], [11], [25], [26], the change in resistance of NiTi was characterized while sweeping the applied current to find the phase transition as shown in Fig. 3(a). A source-measure unit (SMU) instrument (2410, Keithley) was used to apply a current to the NiTi strips and measure the resistance at the same time. The red and blue lines in Fig. 3(a) show the resistance change while increasing the applied current (heating) and decreasing the applied current (cooling), respectively. A sudden change in the resistance was observed at 22 mA while heating which was used as an indicator for the phase transition from martensite to austenite. The steady state T_{avg} was estimated to be 74 °C at 22 mA. A negative temperature coefficient of resistance was observed while decreasing the current from 22 to 14 mA (Fig. 3(a)), indicating the austenite to martensite transition. Three ranges of the applied current were swept which are illustrated with different marker shapes on the plot. The current to resistance plots at different current ranges overlapped each other, showing a consistent phase transition of the NiTi strips.

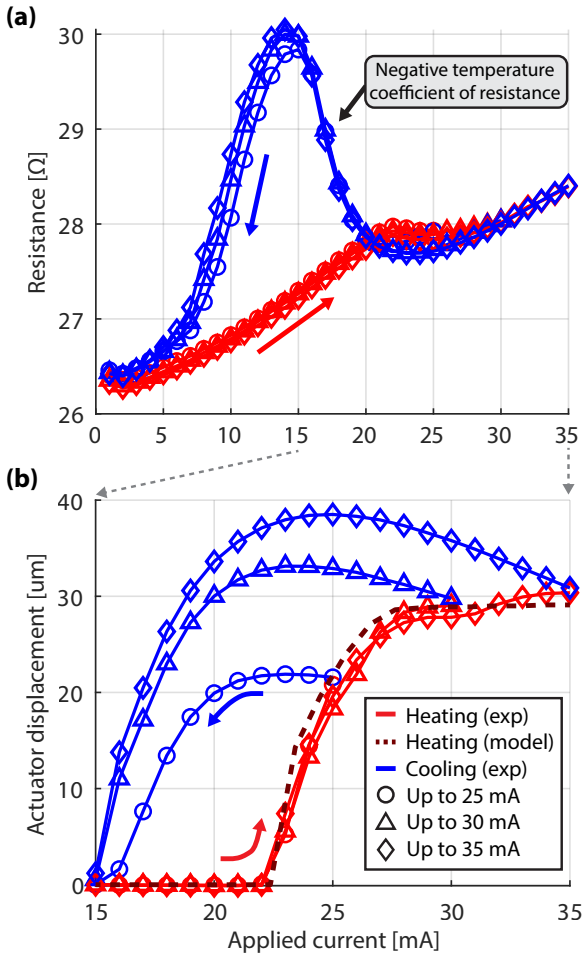

Fig. 3. Characterization results of the thin-film NiTi actuator. (a) The resistance of the NiTi microactuators was measured while sweeping the applied current. (b) The change in the displacement of the NiTi actuator while sweeping the applied current. There was no observable displacement at currents lower than 15 mA. The red line shows the measurement while increasing the current and heating up the actuator, and the blue line shows the measurement while decreasing the current and cooling the actuator.

The actuator displacement was characterized in a similar way as the change in the resistance (Fig. 3(b)). Current was swept with the SMU instrument, and a DSLR camera (D850, Nikon) was mounted over a probestation (S-250-6, Signatone) to record the actuator displacements. Motion analysis

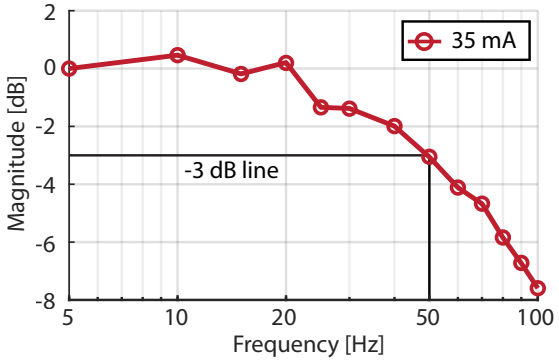

Fig. 4. Frequency response of the thin-film NiTi actuator. The actuator can be operated up to 50 Hz without crossing the -3 dB line.

software (TEMA T2020, Image Systems) was utilized to track the actuator position. An applied current greater than 22 mA was required to overcome the magnetic force between the two permanent magnets and generate actuator displacement. A maximum displacement of 30 µm was achieved with a 35 mA current while heating. The actuator displacement while heating was also predicted by the model which showed a good agreement with the experimetal results. T_{avg} at 35 mA was estimated to be 156 °C from the model. The actuator displacement showed a hysterisis loop similar to the stress-temperature plots shown in [10] which also indicates that the NiTi is undergoing a phase transition. A larger actuator displacement was achieved while cooling, which reached up to 38.5 µm. The change in the material properties of the thin-film NiTi while cooling needs to be further studied to better understand the actuation behavior for practical applications. There were no observable displacements when the applied current was below 15 mA.

Many previously developed thin-film NiTi microactuators used bilayer structures to apply strain to the thin-film NiTi [1]–[4], [10], [11], [27]. However, the stack of materials increases the thermal mass of the actuator slowing down the electrothermally driven actuation. The novel actuator configuration presented in this work utilizes bare NiTi thin film without any extra stacked materials that allows for faster actuation speed. To characterize the frequency response of the actuator, square waves from 0 to 35 mA with 50% duty cycle were applied to the actuator at various frequencies, and a high-speed camera (Mini AX200, Photron) was mounted over the probestation to record videos of the actuator motion. As shown in Fig. 4, the actuator was able to operate up to 50 Hz before crossing the -3 dB line. Even though the actuator in this work used a larger mass of NiTi material for actuation than the authors' previous work on a bilayer NiTi actuator [11], the achievable actuation frequency was an order of magnitude higher.

B. Launcher mechanism characterization

To evaluate the powerful actuation of the thin-film NiTi microactuator, the performance of the launcher mechanism was experimentally evaluated. A salt grain was used for a projectile. The mass of the salt grain was estimated to be 100 µg assuming a cube shape, which was 25% of the mass of the actuator and launcher mechanism combined. Once the salt grain was placed at the tip of the launcher, the actuator was actuated and the side view of the mechanism was recorded with the high-speed camera at 6400 frames per second to analyze the trajectory and velocity of the projectile as shown in Fig. 5(a). Fig. 5(b)-(d) shows the transient behavior of the actuator position (y), launcher angle (θ_2), projectile velocity (v_{proj}), and projectile height (h_{proj}), respectively. The red and blue plots each show the modeled behavior and the experimental result. The experiment was repeated for 3 times, and the shaded area around the data points represents standard deviations between data points. The small deviation indicates a good repeatibility of the mechanism. The electrothermal model estimates that the actuator requires approximately 6.5 ms to heat up and overcome the force between the magnets. Once the mechanism started to move, it took 1.1 ms for the projectile to take off from the launcher, and the model and experimental results showed good agreement in terms of the time required for take-off. The measured projectile take-off velocity (v_{proj}^{to}) was 0.23 m/s that was 47 % of the modeled take-off velocity (0.49 m/s). The main source of discrepancy between the model and experimental result is likely the errors in material properties and the lack of damping in the model (e.g., material damping from NiTi [28] and air damping such as squeeze film damping [29]). In addition, there were minor errors in modeling the kinematics since the flexure joints could not provide pure rotation. For example, α in the launcher mechanism was designed such that θ_2 is at 0° before actuation; however, θ_2 in Fig. 5(a) at 6.2 ms was not exactly at 0°. The amount of energy and power delivered to the projectile by the actuator was 2.65 nJ and 2.40 µW.

To further improve the performance of the launcher mechanism, the actuated mechanism was tested with higher current inputs, as shown in Fig. 6. 5, 10, and 15 % increases in input current were applied and both projectile velocities and heights were measured. The pulse width was adjusted to apply the same amount of energy input to the NiTi actuator and to avoid overheating. Since the higher current heats up the actuator faster, the amount of energy and power that could be delivered within a short time window was increased. When the current was increased by 15 %, the take-off velocity almost doubled to 0.47 m/s.

IV. CONCLUSION

This work presents a novel thin-film NiTi microactuator with a magnetic spring. 3D-printed magnet holders were used to keep two permanent magnets in desired locations, and the magnetic force was utilized as a spring to apply a tensile strain to thin-film NiTi. By leveraging the shape memory effect from NiTi, the actuator could generate a free displacement of 30 µm and an expected blocking force of 8.7 mN. Since this configuration can leverage bare thin-film NiTi with a low thermal mass, an actuation bandwidth up to 50 Hz could be reached.

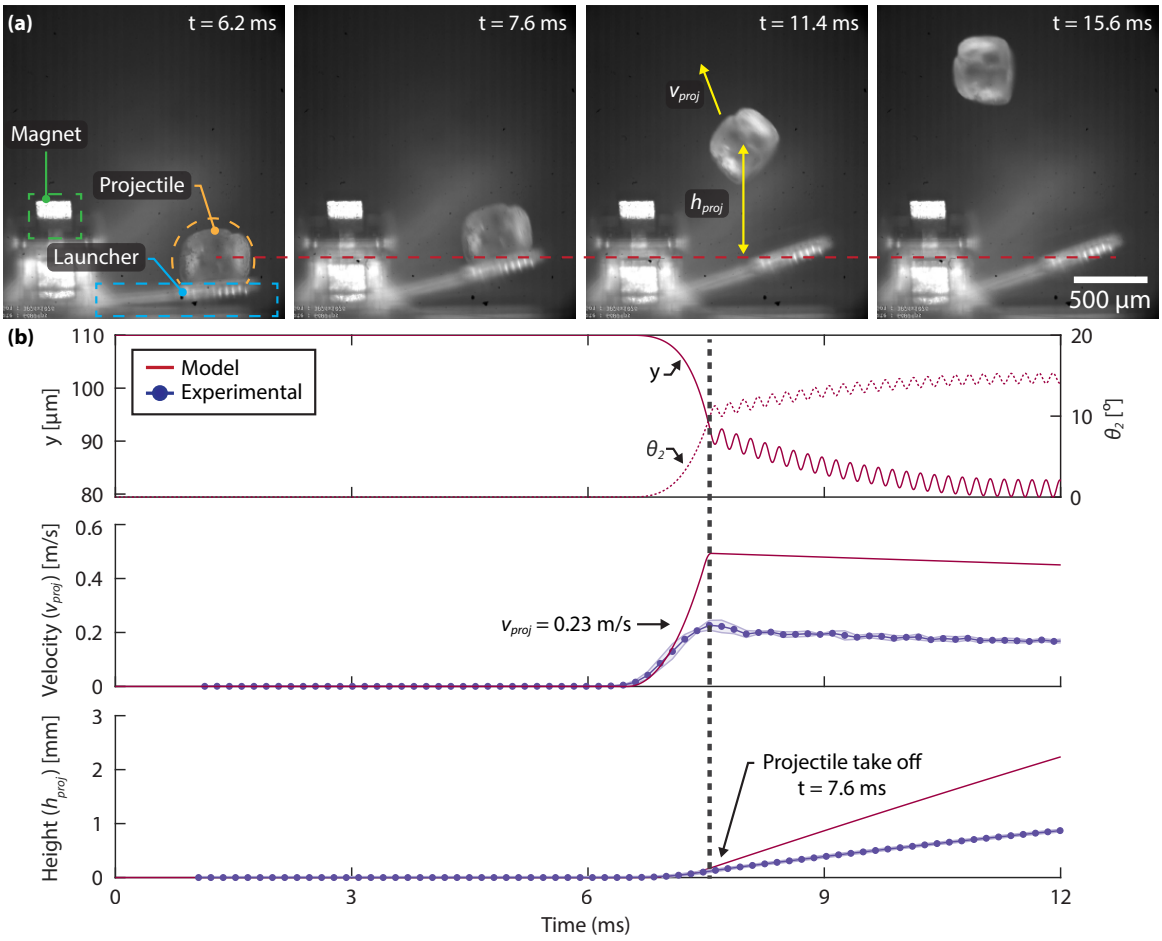

Fig. 5. The launching experiment results (N = 3). A grain of salt was used as a launcher projectile. (a) Video stills of the launcher mechanism and the projectile. (b) The displacement of the actuator (y) over time (solid), and the angle of the launcer (θ_2) over time (dashed). (c) The projectile velocity (v_{proj}) over time. (d) The projectile height (h_{proj}) over time.

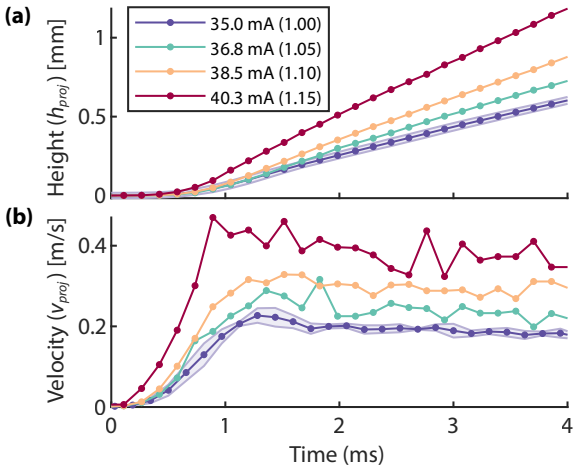

Fig. 6. The launcher performance characterization while varying the current inputs. The values in the parenthesis shows how much the current was changed with respect to 35 mA. (a) The projectile height (h_{proj}) over time. (b) The projectile velocity (v_{proj}) over time.

In addition, a launcher mechanism was designed and integrated to demonstrate the powerful actuation from thin-film NiTi microactuator. A projectile (salt grain) was catapulted from the launcher in 1.1 ms and reached a take-off velocity of 0.23 m/s. The amount of energy and power delivered to the projectile was 2.65 nJ and 2.40 µW, respectively. The dynamic model of the actuator and launcher mechanism was also studied and compared with the experimental results. We also demonstrated how the launcher performance can be significantly improved by a small increase in applied current.

The design of the actuator and the mechanism can be further optimized to improve performance in the future. The current actuator design only leverages approximately 0.6 % of recovery strain on the NiTi film for actuation, which can be further increased up to 5 % by modifying the design of the NiTi strips and the magnetic spring. The link lengths (L_1 and L_2) and the offset (y_i) can also be modified to increase the projectile's take-off velocity. Finally, the analytical model of the actuator and mechanism can be further improved by incorporating damping from the material and environment.

ACKNOWLEDGMENT

The authors would like to thank Dr. Cory Knick and Gabriel Smith at the Army Research Lab for assistance in fabricating the NiTi films.

REFERENCES

[1] C. R. Knick, G. L. Smith, C. J. Morris, and H. A. Bruck, "Rapid and low power laser actuation of sputter-deposited niti shape memory alloy (sma) mems thermal bimorph actuators," *Sensors and Actuators A: Physical*, vol. 291, pp. 48–57, 2019.

[2] P. Krulevitch, A. P. Lee, P. B. Ramsey, J. C. Trevino, J. Hamilton, and M. A. Northrup, "Thin film shape memory alloy microactuators," *Journal of microelectromechanical systems*, vol. 5, no. 4, pp. 270–282, 1996.

[3] J. J. Gill, D. T. Chang, L. A. Momoda, and G. P. Carman, "Manufacturing issues of thin film niti microwrapper," *Sensors and Actuators A: Physical*, vol. 93, no. 2, pp. 148–156, 2001.

[4] C. R. Knick, D. J. Sharar, A. A. Wilson, G. L. Smith, C. J. Morris, and H. A. Bruck, "High frequency, low power, electrically actuated shape memory alloy mems bimorph thermal actuators," *Journal of Micromechanics and Microengineering*, vol. 29, no. 7, p. 075005, 2019.

[5] S.-M. An, J. Ryu, M. Cho, and K.-J. Cho, "Engineering design framework for a shape memory alloy coil spring actuator using a static two-state model," *Smart Materials and Structures*, vol. 21, no. 5, p. 055009, 2012.

[6] R. M. Bena, X.-T. Nguyen, A. A. Calderón, A. Rigo, and N. O. Pérez-Arancibia, "Smarti: a 60-mg steerable robot driven by high-frequency shape-memory alloy actuation," *IEEE Robotics and Automation Letters*, vol. 6, no. 4, pp. 8173–8180, 2021.

[7] J. P. Swensen and A. M. Dollar, "Optimization of parallel spring antagonists for nitinol shape memory alloy actuators," in *2014 IEEE International Conference on Robotics and Automation (ICRA)*. IEEE, 2014, pp. 6345–6349.

[8] M. Moallem and V. A. Tabrizi, "Tracking control of an antagonistic shape memory alloy actuator pair," *IEEE Transactions on control systems technology*, vol. 17, no. 1, pp. 184–190, 2008.

[9] J.-S. Koh and K.-J. Cho, "Omega-shaped inchworm-inspired crawling robot with large-index-and-pitch (lip) sma spring actuators," *IEEE/ASME Transactions On Mechatronics*, vol. 18, no. 2, pp. 419–429, 2012.

[10] C. Velez, D. K. Patel, S. Kim, M. Babaei, C. R. Knick, G. L. Smith, and S. Bergbreiter, "Hierarchical integration of thin-film niti actuators using additive manufacturing for microrobotics," *Journal of Microelectromechanical Systems*, vol. 29, no. 5, pp. 867–873, 2020.

[11] S. Kim and S. Bergbreiter, "3d-printed adaptive microgripper driven by thin-film niti actuators," in *2023 IEEE International Conference on Robotics and Automation (ICRA)*. IEEE, 2023, pp. 5445–5451.

[12] S. Takeuchi and I. Shimoyama, "A three-dimensional shape memory alloy microelectrode with clipping structure for insect neural recording," *Journal of Microelectromechanical systems*, vol. 9, no. 1, pp. 24–31, 2000.

[13] W. L. Benard, H. Kahn, A. H. Heuer, and M. A. Huff, "Thin-film shape-memory alloy actuated micropumps," *Journal of Microelectromechanical systems*, vol. 7, no. 2, pp. 245–251, 1998.

[14] E. Makino, T. Mitsuya, and T. Shibata, "Fabrication of tini shape memory micropump," *Sensors and Actuators A: Physical*, vol. 88, no. 3, pp. 256–262, 2001.

[15] M. A. Woodward and M. Sitti, "Tailored magnetic springs for shape-memory alloy actuated mechanisms in miniature robots," *IEEE Transactions on Robotics*, vol. 35, no. 3, pp. 589–601, 2019.

[16] S. Kim and S. Bergbreiter, "Fabrication and characterization of 3d printed out-of-plane torsional comb-drive actuators for microrobotics," in *2021 21st International Conference on Solid-State Sensors, Actuators and Microsystems (Transducers)*. IEEE, 2021, pp. 6–9.

[17] S. Kim, C. Velez, R. St. Pierre, G. L. Smith, and S. Bergbreiter, "A two-step fabrication method for 3d printed microactuators: Characterization and actuated mechanisms," *Journal of Microelectromechanical Systems*, vol. 29, no. 4, pp. 544–552, 2020.

[18] S. Kim, R. Kubicek, and S. Bergbreiter, "3d-printed electrostatic microactuators for flexible microsystems," *Advanced Functional Materials*, p. 2304991, 2023.

[19] R. St. Pierre, W. Gosrich, and S. Bergbreiter, "A 3d-printed 1 mg legged microrobot running at 15 body lengths per second," in *Solid-State Sensors, Actuators, and Microsystems Workshop, Hilton Head, SC*, vol. 3, 2018.

[20] T. Wang, D. Yang, J. Chen, J. Chow, Y. Hu, K. Hoang, and A. Ansari, "A tetherless microdriller for maneuverability and on-board cargo delivery inside viscoelastic media," in *2022 International Conference on Manipulation, Automation and Robotics at Small Scales (MARSS)*. IEEE, 2022, pp. 1–6.

[21] J. Haringx, "The cross-spring pivot as a constructional element," *Flow, Turbulence and Combustion*, vol. 1, no. 1, pp. 313–332, 1949.

[22] L. Lin and M. Chiao, "Electrothermal responses of lineshape microstructures," *Sensors and Actuators A: Physical*, vol. 55, no. 1, pp. 35–41, 1996.

[23] L. C. Brinson, "One-dimensional constitutive behavior of shape memory alloys: thermomechanical derivation with non-constant material functions and redefined martensite internal variable," *Journal of intelligent material systems and structures*, vol. 4, no. 2, pp. 229–242, 1993.

[24] G. Akoun and J.-P. Yonnet, "3d analytical calculation of the forces exerted between two cuboidal magnets," *IEEE Transactions on magnetics*, vol. 20, no. 5, pp. 1962–1964, 1984.

[25] S. Miyazaki and K. Otsuka, "Deformation and transition behavior associated with ther-phase in ti-ni alloys," *Metallurgical Transactions A*, vol. 17, no. 1, pp. 53–63, 1986.

[26] A. Kumar, D. Singh, and D. Kaur, "Grain size effect on structural, electrical and mechanical properties of niti thin films deposited by magnetron co-sputtering," *Surface and Coatings Technology*, vol. 203, no. 12, pp. 1596–1603, 2009.

[27] M. Babaei, S. Kim, C. Velez, D. K. Patel, and S. Bergbreiter, "Increasing the energy efficiency of niti unimorph actuators with a 3d-printed passive layer," *Journal of Microelectromechanical Systems*, vol. 29, no. 5, pp. 797–803, 2020.

[28] Y. Liu and J. Van Humbeeck, "On the damping behaviour of niti shape memory alloy," *Le Journal de Physique IV*, vol. 7, no. C5, pp. C5–519, 1997.

[29] M. Bao and H. Yang, "Squeeze film air damping in mems," *Sensors and Actuators A: Physical*, vol. 136, no. 1, pp. 3–27, 2007.